Organic Electronics 85 (2020) 105818

Contents lists available at ScienceDirect

Organic Electronics

journal homepage: http://www.elsevier.com/locate/orgel

Stimuli-responsive polymer as gate dielectric for organic transistor sensors

Cut Rullyani [a], Mriganka Singh [a,b], Sheng-Han Li [b], Chao-Feng Sung [c], Hong-Cheu Lin [a,**], Chih-Wei Chu [b,d,e,f,*]

[a] Department of Materials Science and Engineering, National Chiao Tung University, Hsinchu, Taiwan
[b] Research Center for Applied Sciences, Academia Sinica, Taipei, Taiwan
[c] Department of Photonics and Display Institute, National Chiao Tung University, Hsinchu, Taiwan
[d] College of Engineering, Chang Gung University, Guishan District, Taoyuan City, Taiwan
[e] Department of Materials Science and Engineering, National Tsing Hua University, Hsinchu, Taiwan
[f] Research Center for New Generation Photovoltaics, National Central University, Jhong-Li, Taiwan

ARTICLE INFO

Keywords:
Organic thin film transistor
Sensor
Temperature
poly(*N*-isopropylacrylamide) (PNIPAM)

ABSTRACT

Temperature is a characteristic often correlated with environmental and health issues. This paper presents an organic thin film transistor (OTFT) based temperature sensor having a detection range of 30–45 °C, which, therefore, encompasses the human body temperature. The OTFT sensor featured thermosensitive poly(*N*-isopropylacrylamide) (PNIPAM) and pentacene as the gate dielectric and semiconductor, respectively. The PNIPAM film possessed a dielectric constant of 4.2 with very low leakage current density. The OTFT exhibited high electrical performance, with a hole mobility (μ) of 0.90 ± 0.04 $cm^2 V^{-1} s^{-1}$, a threshold voltage (V_{th}) of −15.4 ± 1.16 V, and an on/off ratio of 10^4. Significant changes in the drain current and the values of V_{th} and μ occurred when the temperature of the device was varied within the range 30–45 °C at an interval of 0.5 °C. The operating principle for this temperature sensor was based on the structural transformation of the PNIPAM dielectric and the enhanced charge transport of the pentacene semiconductor upon varying the temperature. Flexible OTFTs fabricated on polyethylene terephthalate substrate displayed hole mobilities as high as 0.39 ± 0.01 $cm^2 V^{-1} s^{-1}$, values of V_{th} of −18.6 ± 0.45, and on/off ratios of 10^2, and were workable for over 100 bending cycles.

1. Introduction

Because of their high sensitivity, biocompatibility, low cost, and simple fabrication, organic thin film transistors (OTFTs) have been studied widely for their use in chemical and physical sensors [1–4]. Such sensors have been developed for, among other things, the detection of gases [5–7], pressure [8], light intensity [9], temperature [10–12], and biological [13] and chemical substances [14]. In addition to pressure and light, heat is another physical parameter that is often measured in sensing applications [10]. Highly sensitive temperature sensors are used in electronic skin [15], in personal health monitoring [16], and in detecting body temperatures in medical settings [10,11]. Among the reported electronic sensors, responsive polymer-based sensing systems are relatively rare [17]. Responsive polymers exhibit reversible or irreversible changes in their physical properties and/or chemical structures in response to external stimuli (e.g., pH; temperature; ionic strength; light; mechanical forces; electric, magnetic, and acoustic fields; specific analysts; external additives) [18–22]. A temperature-responsive polymer will undergo volume phase transitions at certain temperatures—the so-called lower critical solution temperature (LCST) and upper critical solution temperature (UCST)—with rapid changes in the solvation state resulting in chain collapse or expansion [23,24].

Poly(*N*-isopropylacrylamide) (PNIPAM) is a thermoresponsive polymer that undergoes a reversible phase transition upon heating [25]. PNIPAM experiences a coil-to-globule phase transition, followed by phase separation, in water upon heating at temperatures above its LCST (ca. 32 °C) [26,27]. Because of its sharp and reversible transition behavior and an LCST close to human body temperature, PNIPAM has attracted great attention for various applications, especially for those in pharmaceutical and biomedical fields [28,29]. Herein, we report the dielectric properties of PNIPAM and the fabrication of an OTFT-based temperature sensor incorporating thermoresponsive PNIPAM and pentacene as the gate dielectric and semiconductor, respectively. This temperature sensor operated in the range from 30 to 45 °C, thereby

* Corresponding author. Research Center for Applied Sciences, Academia Sinica, Taipei, Taiwan.
** Corresponding author.
E-mail addresses: linhc@cc.nctu.edu.tw (H.-C. Lin), gchu@gate.sinica.edu.tw (C.-W. Chu).

https://doi.org/10.1016/j.orgel.2020.105818
Received 6 April 2020; Received in revised form 18 May 2020; Accepted 20 May 2020
Available online 7 June 2020

encompassing the human body temperature (ca. 36.5–37.5 °C). Our OTFT could sense temperature changes as small as 0.5 °C. A device fabricated on a flexible substrate displayed stable performance for up to 100 bending cycles at a bending radius of 1.5 cm. The concept behind this temperature sensor may be useful for potential applications in flexible and wearable monitoring devices.

2. Results and discussion

The OTFT temperature sensors were fabricated employing a bottom-gate and top-contact configuration, as illustrated in Fig. 1a. The device exhibited p-type performance, as verified from the output and transfer curves in Fig. 1b and c. A pentacene OTFT incorporating a 600-nm-thick PNIPAM dielectric displayed a hole mobility of 0.90 ± 0.04 $cm^2 V^{-1} s^{-1}$, a value of V_{th} of -15.4 ± 1.16 V, and an on/off ratio of 10^4. Fig. 1d presents the chemical structure of the PNIPAM carboxylic acid terminated that was employed in this study. Fig. 1e and f display the surface morphology of the PNIPAM and pentacene films, obtained using AFM in tapping mode. The spin-coated PNIPAM film had a very smooth surface, with root-mean-square (RMS) surface roughness of 0.33 nm. The thermally evaporated pentacene exhibited a typical dendrite structure when grown on top of the PNIPAM dielectric film. The measured RMS surface roughness of the pentacene film was 11.8 nm.

The dielectric properties and gate leakage current are important parameters for any gate dielectric material in an OTFT. To investigate the leakage current and dielectric properties of PNIPAM, a metal–insulator–metal (MIM) structure comprising indium tin oxide (ITO)/PNIPAM/Au was fabricated. Fig. 2a displays the capacitance of the PNIPAM film at various thicknesses, measured in the frequency range from 20 Hz to 1 MHz. The capacitance exhibited a slight frequency-dependence, increasing upon decreasing the film thickness, because the charge in the capacitor was inversely proportional to the distance between the bottom and top electrodes. The measured capacitances for the 750-, 600-, 530-, and 420-nm-thick PNIPAM films at 20 Hz were 439, 657, 753, and 910 pF, respectively. The dielectric constant of the PNIPAM was calculated to be 4.2. Fig. 2b provides a representative plot of the leakage current density with respect to the electric field for the 600-nm PNIPAM film. The leakage current density of the PNIPAM dielectric was less than 1.2×10^{-9} A cm^{-2} within the range from −1.3 to +1.3 MV cm^{-1}.

The responses of the OTFT devices to temperature were investigated by measuring their output and transfer characteristics over the temperature range from 30 to 45 °C. Fig. 3a reveals that the values of I_{DS} increased upon increasing the temperature, from an initial value of −5.7 μA at 30 °C to a final value of −9.8 μA at 45 °C. This inclination was presumably associated with a threshold voltage that shifted to a more positive value upon increasing the temperature, as displayed in Fig. 3b. The value of V_{th} shifted from −16.2 to −9.9 V, as the temperature increased from 30 to 45 °C. Because of the limitations of the equipment used, the lowest applicable increment in temperature was 0.5 °C (Supplementary Fig. S1). To investigate the sensitivity of the OTFT toward the temperature, the electrical performance was measured after varying the temperature; the data are summarized in Fig. 3c and d. The measured values of I_{DS} and μ increased linearly, while the value of V_{th}

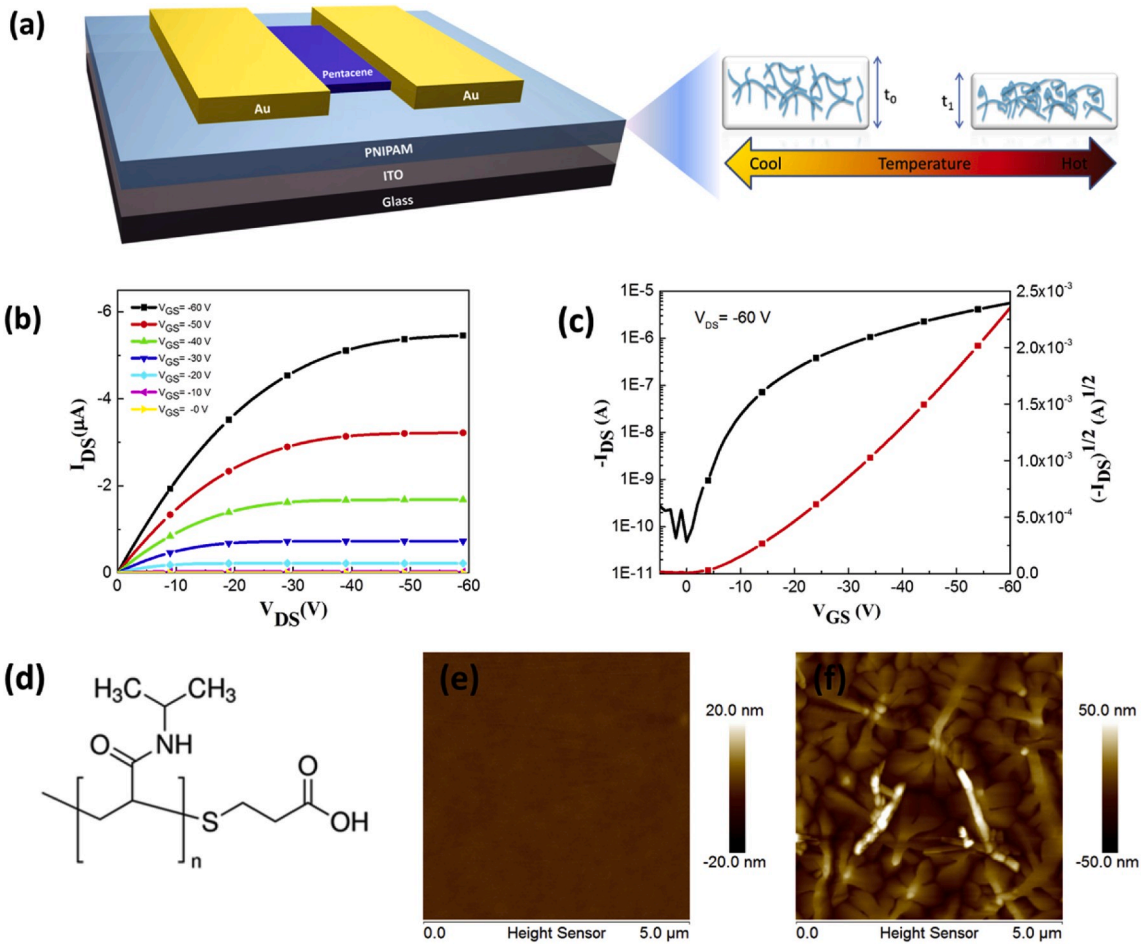

Fig. 1. (a) Schematic representation of a bottom-gate/top-contact OTFT employing 600-nm-thick PNIPAM as a dielectric. (b) Output and (c) transfer characteristics of the pentacene OTFT fabricated on an ITO/glass substrate. (d) Chemical structure of PNIPAM carboxylic acid terminated. (e, f) AFM images (5 μm × 5 μm) of (e) the PNIPAM film on ITO/glass and (f) the pentacene film grown on the PNIPAM dielectric.

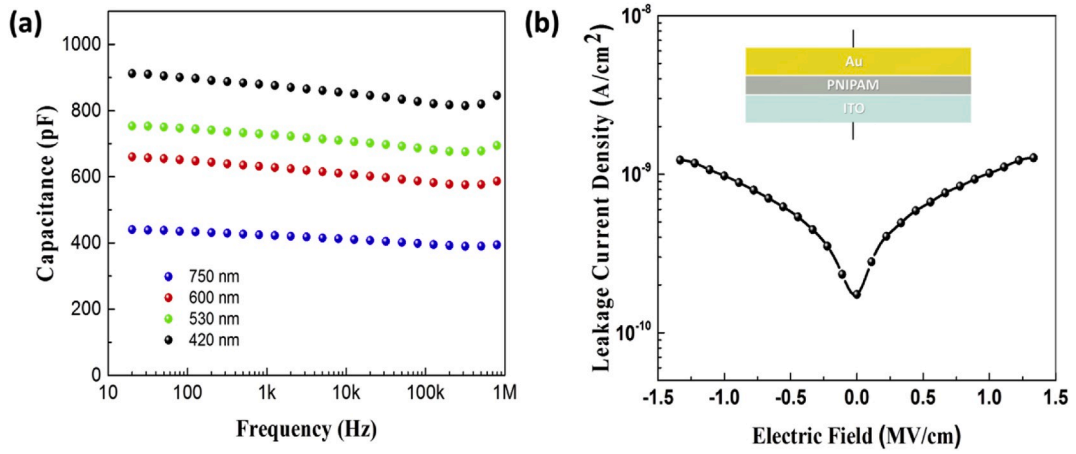

Fig. 2. (a) Capacitance of PNIPAM films of various thicknesses, measured at frequencies from 20 Hz to 1 MHz. (b) Leakage current density of a 600-nm PNIPAM dielectric, measured under electric fields varying from −1.3 to 1.3 MV cm^{-1}.

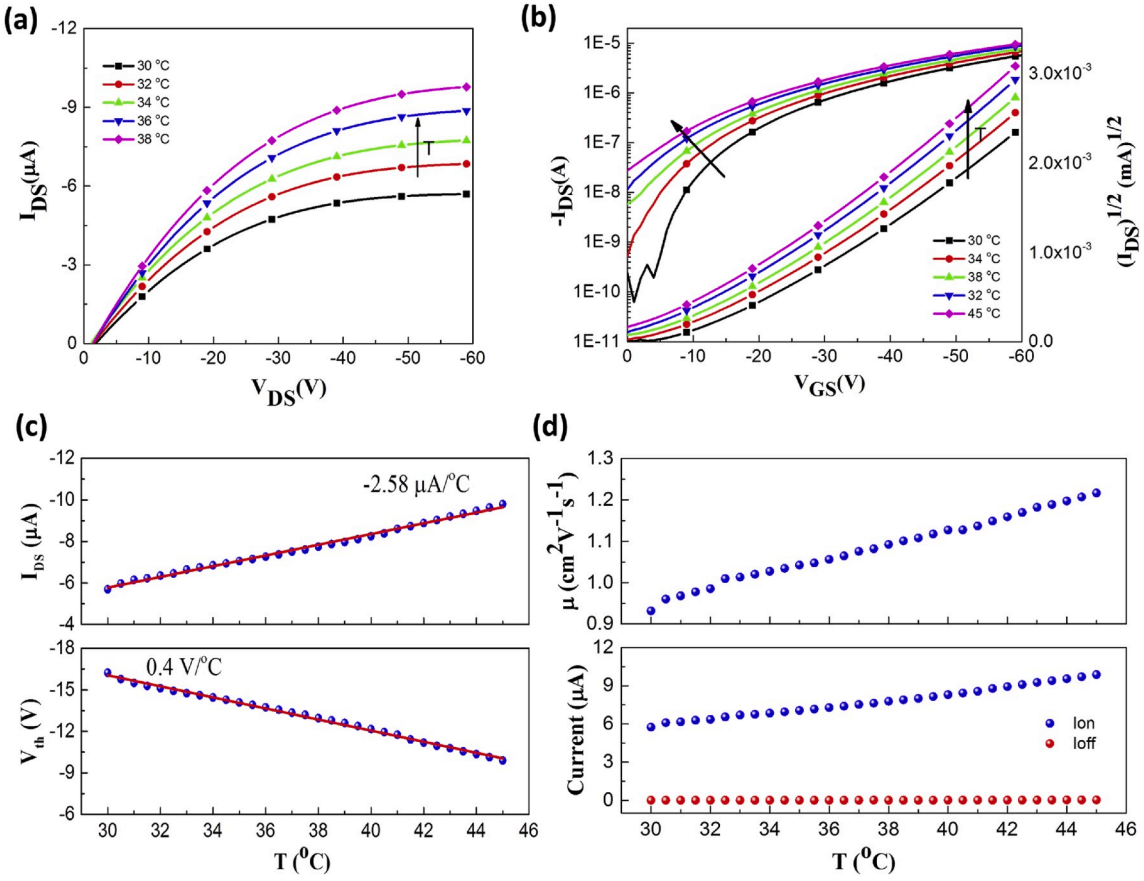

Fig. 3. Temperature-dependent (a) output and (b) transfer curves of pentacene OTFTs measured at a value of V_{DS} of −60 V upon heating from 30 to 45 °C. (c) Values of I_{DS} and V_{th} and (d) mobility and on/off current plotted with respect to temperature.

decreased linearly, upon increasing the temperature. The temperature coefficients of I_{DS} and V_{th}, obtained from linear fitting of the I_{DS} and V_{th} data, were −2.58 μA/°C and 0.4 V/°C, respectively. The on and off currents also increased as a result of increasing temperature. The change in the off current was on the order of nanoamperes; it cannot be observed clearly in Fig. 3d because it was much smaller than the change in the on current, which was in the microampere regime. Supplementary Fig. S2 presents a plot of the off current with respect to temperature on the nanoampere scale. We suspected that the changes in electrical performance were correlated with the enhanced thermal transport properties of pentacene and the conformational change of the PNIPAM dielectric upon heating. In addition, we suspected that the PNIPAM dielectric might form a better interface with the pentacene semiconductor when heated [30].

To acquire a deeper understanding of the role of the PNIPAM dielectric, OTFTs incorporating SiO_2 and PMMA as dielectric materials were also fabricated for comparison. As displayed in Supplementary Fig. S3, the fabricated devices containing SiO_2 and PMMA as dielectrics also exhibited increases in the values of mobility, I_{DS} and shifts in the values of V_{th}, but they were not as significant as those observed for the

OTFT incorporating the PNIPAM dielectric. In the case of SiO_2, the value of mobility increased from an initial mobility of 0.085 $cm^2\ V^{-1}\ s^{-1}$ to a final current of 0.093 $cm^2\ V^{-1}\ s^{-1}$ upon heating from 30 to 60 °C. A similar trend was observed for the OTFT incorporating the PMMA dielectric: here, the value of mobility increased correspondingly from 0.031 to 0.035 $cm^2\ V^{-1}\ s^{-1}$. A summary of temperature-dependent mobility plotted with respect to temperature, as shown in Supplementary Fig. S4. Thus, charge transport through the pentacene semiconductor was indeed improved upon increasing the temperature [31,32], with PNIPAM playing an important role in enhancing the temperature-sensitivity of the OTFT sensor. The change in mobility vs. reciprocal temperature in our OTFT incorporating the various dielectrics materials, as shown in Supplementary Fig. S5a. As we can see the temperature, dependent mobility exhibited an Arrhenius relationship [32]. The slopes of curves from supplementary Fig. S5a, the activation energy E_a was calculated at 3.19, 4.78, and 17.8 meV for various dielectrics materials SiO_2, PMMA and PNIPAM, respectively, as shown in Supplementary Fig. S5b. To confirm the influence of PNIPAM on the sensing performance, a ITO/PNIPAM/Au sandwich structure was fabricated; its capacitance was measured at various temperatures. Fig. 4a presents the dependency of the capacitance on temperature when the structure containing 600-nm-thick PNIPAM was heated from 25 to 45 °C and measured at frequencies in the range from 20 Hz to 1 MHz. Temperature rise led to an increase in capacitance and, therefore, an increase in dielectric permittivity. Fig. 4b presents the capacitance of the PNIPAM film measured at 20 Hz while heating from 25 to 45 °C. The measured capacitance increased linearly with respect to temperature: from 657 to 688 pF upon increasing the temperature from 25 to 45 °C. Temperature-dependent current measured for up to six heating cycle, as shown in Supplementary Fig. S6. The phenomenon of capacitance and permittivity increases may be related to the PNIPAM backbone chain collapsing as the temperature increased [33,34]. PNIPAM contains both hydrophobic and hydrophilic groups that form hydrogen bonds with water molecules [26]. Increasing the temperature disrupts the hydrogen bonds between the water molecules and the hydrophobic moieties of PNIPAM, leading to a conformational change from a linear to a globular state [35–37]. This transformation from linear to globular occurs with a shrinking of volume that also affects the thickness of a PNIPAM film [38,39]. Our results confirmed that the enhanced sensing sensitivity of the OTFT sensor was governed by changes in the structure of the PNIPAM dielectric, as well as the improved thermal transport properties of the pentacene semiconductor. The comparison between OTFT based temperature sensors, as shown in Supplementary Table S1.

To measure the spatial temperature gradients, a 3 × 3 transistor array was fabricated on a 2 × 2 cm^2 ITO/glass substrate (Fig. 5a). Fig. 5b presents the distribution of values of I_{DS} of the individual OTFTs in the array. The insignificant variations in color indicated that all of the devices maintained almost uniform values of I_{DS}, with highest and lowest values of −5.79 and −5.19 μA, respectively. The slight variations in electrical performance of the OTFTs within the array were presumably caused by differences in the crystallinity of the organic semiconducting layer [40]. Supplementary Fig. S7 presents the I_{DS}, V_{th} and μ of the nine devices within the 3 × 3 transistor array. The spatial temperature mapping was determined by heating one corner of the glass substrate to 45 °C; the electrical performance of each transistor was recorded and plotted in two dimensions, with the intensity of the color representing the measured performance. Fig. 5c–e display the values of I_{DS}, the mobility, and the gradient in the values of V_{th} while heating the upper corner of the substrate. The device closest to the heating source exhibited the highest values of I_{DS} and μ and the largest shift in the value of V_{th}; the devices next to it were also slightly affected.

Fig. 6a displays a photograph of a flexible OTFT fabricated on a polyethylene terephthalate (PET) substrate. The flexible OTFTs exhibited a charge carrier mobility of 0.39 ± 0.01 $cm^2\ V^{-1}\ s^{-1}$, a value of V_{th} of −18.6 ± 0.45 V, and an on/off ratio of 10^2, as extracted from the output and transfer curves in Fig. 6b and c. The electrical performance of the devices fabricated on the flexible substrates was poorer than that of those fabricated on the ITO/glass substrate, presumably because the adhesion and uniformity of the PNIPAM film on the PET substrate affected the growth of the semiconductor layer. The flexibility of the device was evaluated through cyclic bending at a radius of 1.5 cm. Fig. 6d plots the mobility, values of V_{th}, and on/off current of the flexible device as a function of bending number. The devices exhibited stable performance with no significant shifts in their transfer curves, as exemplified by the values of V_{th} increasing by 6.17% and mobility decreasing by 3.51% after 100 bending cycles.

3. Conclusions

We have fabricated OTFTs incorporating a thermoresponsive PNIPAM dielectric as a flexible sensing platform. The devices displayed a carrier mobility of 0.90 ± 0.04 $cm^2\ V^{-1}\ s^{-1}$, a value of V_{th} of −15.4 ± 1.16 V, and an on/off ratio of 10^4 at a gate voltage of −60 V. The temperature-dependence of the characteristics were governed by (i) a linear-to-globular transformation of PNIPAM, causing the capacitance and permittivity to increase in the gate dielectric, and (ii) thermally activated charge transport in the pentacene semiconductor. A device prepared on a flexible substrate exhibited a carrier mobility of 0.39 ± 0.01 $cm^2\ V^{-1}\ s^{-1}$, a value of V_{th} of −18.6 ± 0.45 V, and an on/off ratio of 10^2. This flexible OTFT displayed stable performance for more than 100 bending cycles. This proof-of-concept study suggests the potential of using smart polymer dielectrics in flexible and wearable monitoring

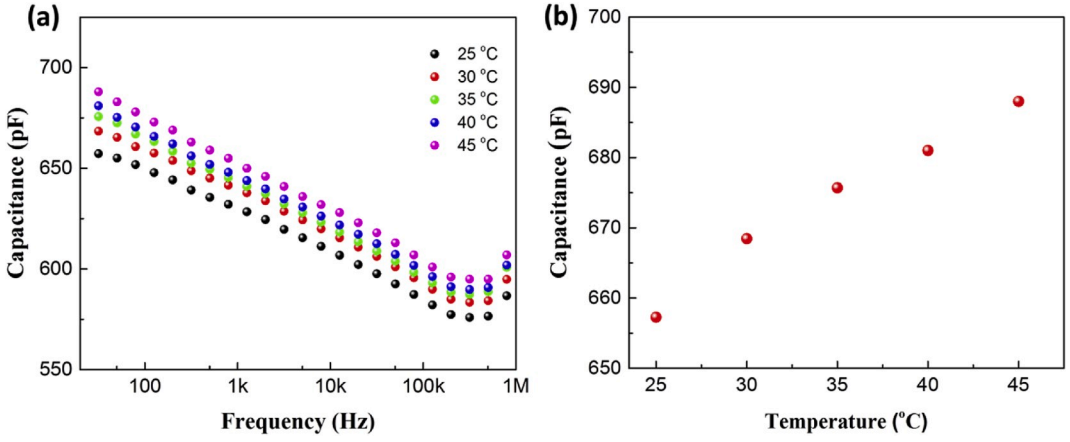

Fig. 4. (a) Capacitance of a 600-nm PNIPAM film, measured from 20 Hz to 1 MHz at various temperatures. (b) Capacitance of PNIPAM measured at 20 Hz, upon heating from 25 to 45 °C.

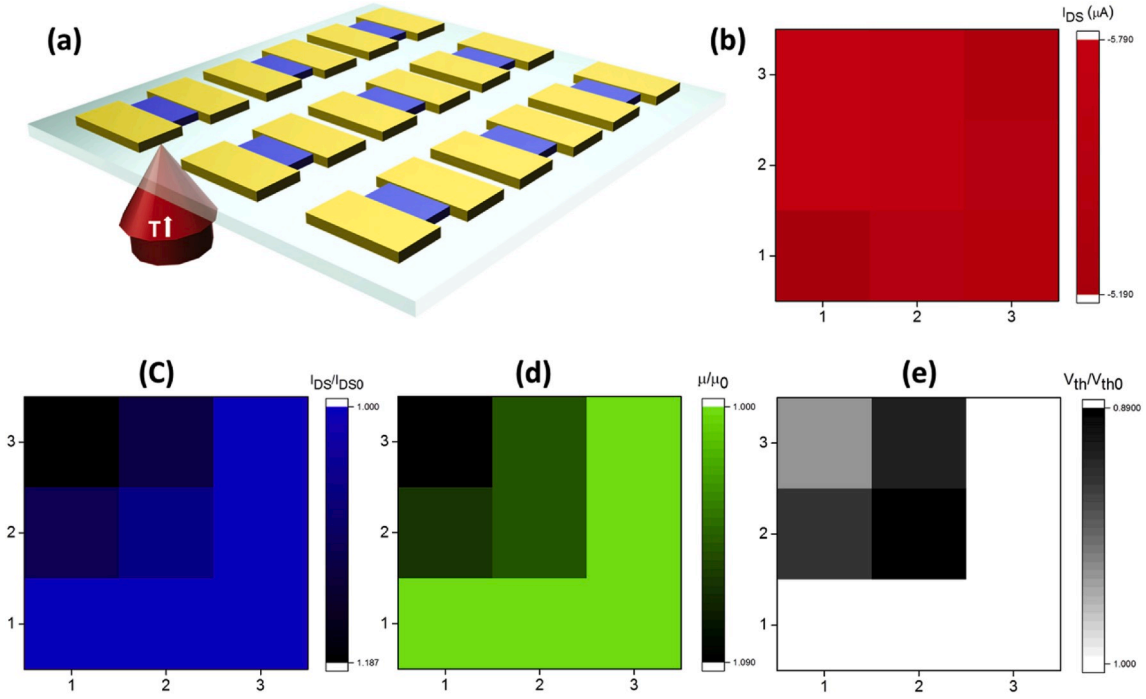

Fig. 5. (a) Illustration of the 3 × 3 transistor array; one device in the upper corner was heated at 45 °C. (b) Dispersion of the values of I_{DS} of nine devices before heating; (c–e) corresponding values of (c) $I_{DS}/I_{DS0,}$ (d) $\mu/\mu_{0,}$ and (e) V_{th}/V_{th0} upon heating.

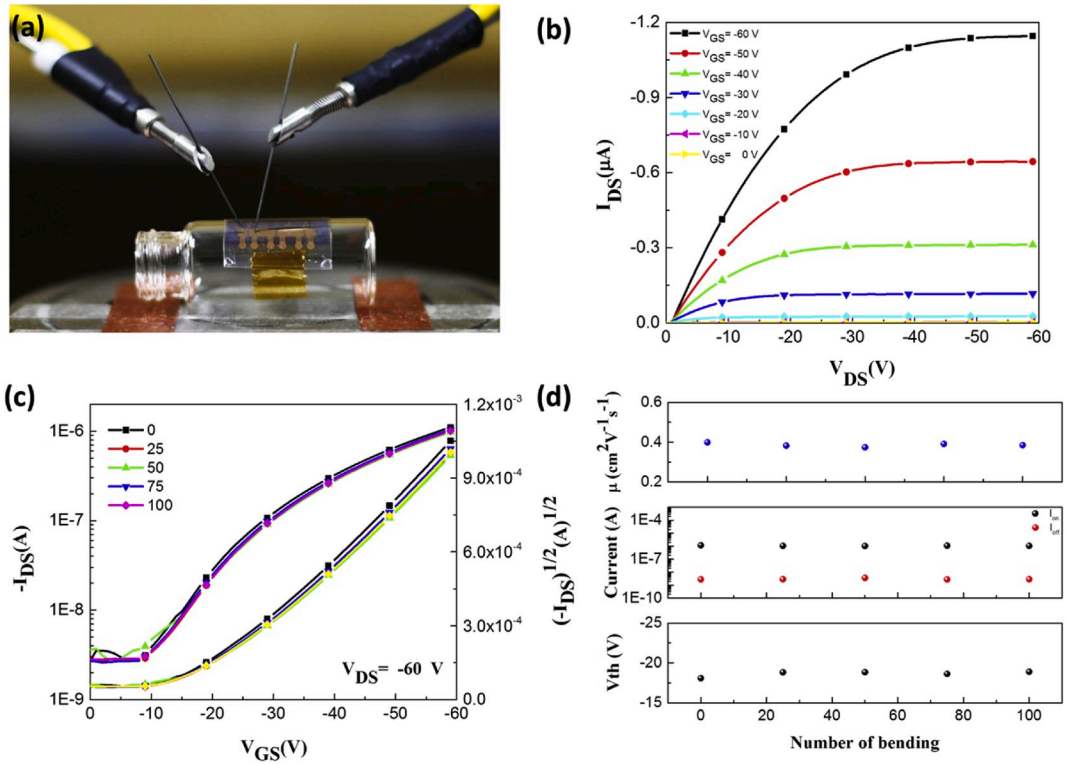

Fig. 6. (a) Photograph of a flexible OTFT incorporating a 1150-nm-thick PNIPAM dielectric. (b) Output and (c) transfer characteristics of an OTFT fabricated on a PET substrate. (d) Changes in the mobility, on/off current, and value of V_{th} after 100 cycles of bending at a radius of 1.5 cm.

devices.

4. Experimental section

4.1. Materials

Pentacene (P1802, assay 99%) and PNIPAM carboxylic acid

terminated (average M_n 10000) were purchased from Sigma–Aldrich and used without further purification.

4.2. Device fabrication

An indium tin oxide (ITO) coated glass substrate was cleaned with the usual procedure followed by DI water, detergent, acetone, and IPA for each 20 min and later UV-Ozone cleaner (30 min) used before to fabricate the bottom-gate top-contact OTFTs. A gate dielectric PNIPAM solution was prepared 15 wt% in DI water. A thin layer of PNIPAM was spin-coated on an ITO substrate by spin speed 2000 rpm for 30 s and further annealed the film at 85 °C for 40 min. The thermal deposition was used to deposit the active layer (pentacene, 70 nm) and metallic electrodes (source and drain, 40 nm). The electrodes deposited through the shadow mask having a dimension of channel width and channel length of 200 μm and 2000 μm, respectively. A similar procedure has been followed to fabricate the flexible devices on polyethylene terephthalate (PET) substrates via two times of spin coating (1000 rpm, 30 s) a PNIPAM dielectric layer.

4.3. Device characterization

The carrier mobility of the OTFT devices in the saturated regime was calculated by using equation (1).

$$I_D = \left(\frac{W}{2L}\right) C_i \mu (V_G - V_T)^2 \quad (1)$$

where I_D is the drain current in the saturated regime; W and L are the channel width and length, respectively; μ is the carrier mobility; C_i is the capacitance (per unit area) of the gate dielectric layer; and V_G and V_T are the gate and threshold voltages, respectively.

To measure the leakage current and capacitance in OTFT device, MIM capacitors were fabricated using structure glass/ITO/PNIPAM/Au. The thickness of dielectric layer varying using various spin speed from 1000 rpm to 4000 rpm and baked film at 85 °C for 40 min. The dielectric constant was calculated by using equation (2).

$$k = \frac{Cd}{\varepsilon_0 A} \quad (2)$$

where C is the capacitance, ε_0 is the vacuum permittivity, d is the thickness of the dielectric layer, and A is the active area (= 0.1 cm^2) of the capacitor.

The dielectric layer thickness was measured using a Bruker Dektak profilometer. Morphology of OTFTs devices was measured using atomic force microscopy from Bruker. The capacitance of OTFTs was measured using a Solartron SI 1260 impedance/gain phase analyzer.

To calculate the mobility of OTFTs devices, we have consider the 20 Hz frequency. The electrical measurement of the OTFTs devices was measured using a Keithley 4200 semiconductor analyzer. The OTFT sensors were tested by pre-heat (40 s) and again measured the electrical performances. Bending tests of flexible devices were performed at a bending radius of 1.5 cm; changes in the electrical performance were measured in various cycles. All the electrical measurement performed under the N_2-filled environment.

Declaration of competing interest

The authors have no competing interests.

Acknowledgments

This study was funded by the Ministry of Science and Technology (MOST) in Taiwan (via MOST 107-2221-E-001 -007-MY3, MOST106-2113-M-009-012-MY3, MOST107-2221-E-009-043-MY2, and MOST108-3017-F-009-004) and the Center for Emergent Functional Matter Science of National Chiao Tung University from The Featured Areas Research Center Program within the framework of the Higher Education Sprout Project by the Ministry of Education (MOE) in Taiwan.

Appendix A. Supplementary data

Supplementary data related to this article can be found at https://doi.org/10.1016/j.orgel.2020.105818.

References

[1] J.T. Mabeck, G.G. Malliaras, Anal. Bioanal. Chem. 384 (2006) 343–353.
[2] P. Lin, F. Yan, Adv. Mater. 24 (2012) 34–51.
[3] Y.H. Lee, M. Jang, M.Y. Lee, O.Y. Kweon, J.H. Oh, Inside Chem. 3 (2017) 724–763.
[4] D. Elkington, N. Cooling, W. Belcher, P. Dastoor, X. Zhou, Electronics 3 (2014) 234.
[5] W. Huang, X. Zhuang, F.S. Melkonyan, B. Wang, L. Zeng, G. Wang, S. Han, M. J. Bedzyk, J. Yu, T.J. Marks, A. Facchetti, Adv. Mater. 29 (2017), 1701706 n/a.
[6] B. Nketia-Yawson, A.R. Jung, Y. Noh, G.-S. Ryu, G.D. Tabi, K.-K. Lee, B. Kim, Y.-Y. Noh, ACS Appl. Mater. Interfaces 9 (2017) 7322–7330.
[7] C. Zhang, P. Chen, W. Hu, Chem. Soc. Rev. 44 (2015) 2087–2107.
[8] Y. Zang, H. Shen, D. Huang, C.-A. Di, D. Zhu, Adv. Mater. 29 (2017), 1606088 n/a.
[9] K.E. Lee, J.U. Lee, D.G. Seong, M.-K. Um, W. Lee, J. Phys. Chem. C 120 (2016) 23172–23179.
[10] X. Ren, P.K.L. Chan, J. Lu, B. Huang, D.C.W. Leung, Adv. Mater. 25 (2013) 1291–1295.
[11] X. Ren, K. Pei, B. Peng, Z. Zhang, Z. Wang, X. Wang, P.K.L. Chan, Adv. Mater. 28 (2016) 4832–4838.
[12] M. Song, J. Seo, H. Kim, Y. Kim, ACS Omega 2 (2017) 4065–4070.
[13] T. Minamiki, T. Minami, P. Koutnik, P. Anzenbacher, S. Tokito, Anal. Chem. 88 (2016) 1092–1095.
[14] B. Wang, P. Sonar, S. Manzhos, H. Haick, Sensor. Actuator. B Chem. 251 (2017) 49–56.
[15] X. Wu, Y. Ma, G. Zhang, Y. Chu, J. Du, Y. Zhang, Z. Li, Y. Duan, Z. Fan, J. Huang, Adv. Funct. Mater. 25 (2015) 2138–2146.
[16] T. Yokota, Y. Inoue, Y. Terakawa, J. Reeder, M. Kaltenbrunner, T. Ware, K. Yang, K. Mabuchi, T. Murakawa, M. Sekino, W. Voit, T. Sekitani, T. Someya, Proc. Natl. Acad. Sci. Unit. States Am. 112 (2015) 14533–14538.
[17] J. Hu, S. Liu, Macromolecules 43 (2010) 8315–8330.
[18] A. Gandhi, A. Paul, S.O. Sen, K.K. Sen, Asian J. Pharm. Sci. 10 (2015) 99–107.
[19] B. Priya, P. Viness, E.C. Yahya, C.d.T. Lisa, Biomed. Mater. 4 (2009), 022001.
[20] M. Wei, Y. Gao, X. Li, M.J. Serpe, Polym. Chem. 8 (2017) 127–143.
[21] A. Ahiabu, M.J. Serpe, ACS Omega 2 (2017) 1769–1777.
[22] E. Cabane, X. Zhang, K. Langowska, C.G. Palivan, W. Meier, Biointerphases 7 (2012) 9.
[23] Y.-J. Kim, Y.T. Matsunaga, J. Mater. Chem. B 5 (2017) 4307–4321.
[24] R. Hoogenboom, 2 - temperature-responsive polymers: properties, synthesis and applications, in: M.R. Aguilar, J. San Román (Eds.), Smart Polymers and Their Applications, Woodhead Publishing, 2014, pp. 15–44.
[25] K. Kubota, S. Fujishige, I. Ando, Polym. J. 22 (1990) 15.
[26] M.H. Futscher, M. Philipp, P. Müller-Buschbaum, A. Schulte, Sci. Rep. 7 (2017) 17012.
[27] T. Tada, T. Hirano, K. Ute, Y. Katsumoto, T.-A. Asoh, T. Shoji, N. Kitamura, Y. Tsuboi, J. Phys. Chem. B 120 (2016) 7724–7730.
[28] M.A. Ward, T.K. Georgiou, Polymers 3 (2011) 1215.
[29] N. Vanparijs, L. Nuhn, B.G. De Geest, Chem. Soc. Rev. 46 (2017) 1193–1239.
[30] J.H. Oh, S.Y. Hong, H. Park, S.W. Jin, Y.R. Jeong, S.Y. Oh, J. Yun, H. Lee, J.W. Kim, J.S. Ha, ACS Appl. Mater. Interfaces 10 (2018) 7263–7270.
[31] S. Jung, T. Ji, V.K. Varadan, Appl. Phys. Lett. 90 (2007), 062105.
[32] D. Guo, S. Ikeda, K. Saiki, H. Miyazoe, K. Terashima, J. Appl. Phys. 99 (2006), 094502.
[33] B. Sun, Y. Lin, P. Wu, H.W. Siesler, Macromolecules 41 (2008) 1512–1520.
[34] S. Sun, J. Hu, H. Tang, P. Wu, J. Phys. Chem. B 114 (2010) 9761–9770.
[35] F. Gómez-Galván, T. Lara-Ceniceros, H. Mercado-Uribe, Meas. Sci. Technol. 23 (2012), 025602.
[36] M. Yang, C. Liu, Y. Lian, K. Zhao, D. Zhu, J. Zhou, Soft Matter 13 (2017) 2663–2676.
[37] I. Bischofberger, D.C.E. Calzolari, P. De Los Rios, I. Jelezarov, V. Trappe, Sci. Rep. 4 (2014) 4377.
[38] M. Li, B. Bresson, F. Cousin, C. Fretigny, Y. Tran, Langmuir 31 (2015) 11516–11524.
[39] T. Masuda, T. Kajisa, A.M. Akimoto, A. Fujita, K. Nagase, T. Okano, T. Sakata, R. Yoshida, RSC Adv. 7 (2017) 34517–34521.
[40] K. Fukuda, Y. Takeda, M. Mizukami, D. Kumaki, S. Tokito, Sci. Rep. 4 (2014) 3947.